12-1-2011

Magnetic order in GdBiPt studied by x-ray resonant magnetic scattering

Andreas Kreyssig
Iowa State University and Ames Laboratory, kreyssig@ameslab.gov

M. G. Kim
Iowa State University and Ames Laboratory

J. W. Kim
Argonne National Laboratory

D. K. Pratt
Iowa State University and Ames Laboratory

S. M. Sauerbrei
Iowa State University and Ames Laboratory

See next page for additional authors

Magnetic order in GdBiPt studied by x-ray resonant magnetic scattering

Abstract

Rare-earth (R) half-Heusler compounds RBiPt exhibit a wide spectrum of interesting ground states. We have employed x-ray resonant magnetic scattering to elucidate the microscopic details of the magnetic structure in GdBiPt below TN=8.5 K. Experiments at the Gd L2 absorption edge show that the Gd moments order in an antiferromagnetic stacking along the cubic diagonal [111] direction, satisfying one of the requirements for an antiferromagnetic topological insulator as proposed previously, where both time-reversal symmetry and lattice translational symmetry are broken, but their product is conserved.

Disciplines

Condensed Matter Physics

Comments

This article is published as Kreyssig, A., M. G. Kim, J. W. Kim, D. K. Pratt, S. M. Sauerbrei, S. D. March, G. R. Tesdall et al. "Magnetic order in GdBiPt studied by x-ray resonant magnetic scattering." *Physical Review B* 84, no. 22 (2011): 220408. DOI: 10.1103/PhysRevB.84.220408. Posted with permission.

Authors

Andreas Kreyssig, M. G. Kim, J. W. Kim, D. K. Pratt, S. M. Sauerbrei, S. D. March, G. R. Tesdall, Sergey L. Bud'ko, Paul C. Canfield, Robert J. McQueeney, and Alan I. Goldman

PHYSICAL REVIEW B **84**, 220408(R) (2011)

Magnetic order in GdBiPt studied by x-ray resonant magnetic scattering

A. Kreyssig,[1] M. G. Kim,[1] J. W. Kim,[2] D. K. Pratt,[1] S. M. Sauerbrei,[1] S. D. March,[1] G. R. Tesdall,[1] S. L. Bud'ko,[1] P. C. Canfield,[1] R. J. McQueeney,[1] and A. I. Goldman[1]

[1]*Ames Laboratory, US Department of Energy and Department of Physics and Astronomy, Iowa State University, Ames, Iowa 50011, USA*

[2]*Advanced Photon Source, Argonne National Laboratory, Argonne, Illinois 60439, USA*

(Received 15 September 2011; revised manuscript received 29 October 2011; published 21 December 2011)

Rare-earth (R) half-Heusler compounds RBiPt exhibit a wide spectrum of interesting ground states. We have employed x-ray resonant magnetic scattering to elucidate the microscopic details of the magnetic structure in GdBiPt below $T_N = 8.5$ K. Experiments at the Gd L_2 absorption edge show that the Gd moments order in an antiferromagnetic stacking along the cubic diagonal [111] direction, satisfying one of the requirements for an antiferromagnetic topological insulator as proposed previously, where both time-reversal symmetry and lattice translational symmetry are broken, but their product is conserved.

DOI: 10.1103/PhysRevB.84.220408 PACS number(s): 75.25.−j, 75.50.Ee, 73.20.−r

Heusler and half-Heusler compounds exhibit a wide spectrum of interesting ground states.[1] The rare-earth (R) half-Heusler compounds RBiPt feature magnetic ordering,[2] superconductivity (LaBiPt, YBiPt),[3,4] and heavy-fermion behavior (YbBiPt).[5] Although the low-temperature ground states of the RBiPt system (for R = Ce, Nd, Sm, Gd, Tb, Dy, Ho, Er, Tm, and Yb) have been characterized as antiferromagnetic through thermodynamic and transport measurements, there have been few magnetic structure determinations for this series.[6] GdBiPt has the highest T_N of the series at ∼8.5 K (Ref. 2) and, since the orbital angular moment $L = 0$ for the S-state Gd ion, the magnetic structure in the absence of crystalline electric field effects and symmetry-changing magnetoelastic effects may be directly investigated. GdBiPt, therefore, provides an important starting point for investigations of the magnetic structure of RBiPt compounds. However, the high neutron-absorption cross section for naturally occurring Gd is problematic for conventional magnetic diffraction experiments.

Recently, the Heusler and half-Heusler compounds have also been subject to intense scrutiny because of their potential as a topological insulator (TI) with tunable electronic properties.[7–10] The discovery of three-dimensional topological-insulating states in binary alloys ($Bi_{1-x}Sb_x$)[11,12] and compounds (Bi_2Se_3, Bi_2Te_3, Sb_2Te_3),[13–15] which feature an insulating gap in the bulk but with topologically protected conducting states on the surfaces or edges, has opened an exciting frontier for fundamental condensed-matter physics research.[16] As pointed out in several papers, the properties of this class of materials offer potential for technological breakthroughs in quantum computing and magnetoelectronic applications.[16–18] Over the past year, attention has turned toward investigations of phenomena that arise when TIs also manifest, or are in close proximity to, other phenomena, including magnetic order and superconductivity.[16,18–20] Mong *et al.*[20] have proposed that GdBiPt may provide a realization of an antiferromagnetic topological insulator (AFTI), where both time-reversal symmetry and lattice translational symmetry are broken, but their product is conserved. The AFTI state may be derived from magnetic ordering in a preexisting strong TI (model A in Ref. 20). Given previous angle-resolved photoemission spectroscopy (ARPES) measurements[21] above T_N, which do not find direct evidence for band inversion in GdBiPt, it seems unlikely that GdBiPt is itself a strong TI. However, the AFTI state may be alternatively derived for specific antiferromagnetic ordering schemes that induce spin-orbit coupling in the system (model B in Ref. 20). Predictions for this class of TI include gapped states on some surfaces, gapless states on others, and one-dimensional metallic states along step edges on the gapped surfaces.[20]

Here we describe the magnetic order of GdBiPt below $T_N = 8.5$ K determined by x-ray resonant magnetic scattering (XRMS) at the Gd L_2 absorption edge. GdBiPt crystallizes in the MgAgAs-type structure (cubic space group $F\bar{4}3m$, $a = 6.68$ Å with Gd, Bi, and Pt at the 4c, 4d and 4a sites, respectively; see Fig. 1).[22,23] The structure can be viewed as three sets of elementally pure, interpenetrating face-centered-cubic lattices. We find that the commensurate magnetic order doubles the cubic unit cell along the diagonal [111] direction, characterized by a propagation vector $\mathbf{q}_m = (\frac{1}{2}\frac{1}{2}\frac{1}{2})$, so that alternating ferromagnetic (111) planes of Gd are antiferromagnetically coupled along the [111] direction. This structure is quite similar to the model B magnetic structure for an AFTI via spin-orbit coupling as described by Mong *et al.*,[20] but we find that the moment direction in GdBiPt is not parallel to the magnetic propagation vector as is found, for example, in MnSbCu (Ref. 24) or CeBiPt.[6]

Single crystals of GdBiPt were solution grown using a Bi flux and emerged with sizable facets perpendicular to the [001] direction and smaller facets perpendicular to [111]. High-purity Gd (obtained from Ames Laboratory), Pt, and Bi were placed in an alumina crucible in the ratio Gd : Pt : Bi = 3 : 3 : 94, sealed in a silica ampule, and slowly cooled from 1170 to 600 °C over 200 h. At 600 °C, the excess Bi solution was decanted from the GdBiPt crystals.[25] The dimensions of the single crystal studied in the XRMS measurements were ∼3 × 3 × 2 mm^3 with a large as-grown facet perpendicular to [001]. The measured mosaicity of the crystal was less than 0.01° full width at half maximum (FWHM), attesting to the high quality of the sample. The XRMS experiment was performed on the 6ID-B beamline at the Advanced Photon Source at the Gd L_2 edge (E = 7.934 keV). The incident radiation was linearly polarized perpendicular to the vertical scattering plane (σ polarized) with a beam size of 0.5 mm (horizontal) × 0.2 mm (vertical).

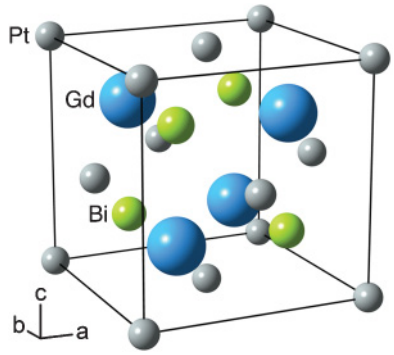

FIG. 1. (Color online) Crystal structure of GdBiPt.

In this configuration, dipole resonant magnetic scattering rotates the plane of linear polarization into the scattering plane (π polarization). For some of the measurements, pyrolytic graphite PG (006) was used as a polarization analyzer to suppress the charge and fluorescence background relative to the magnetic scattering signal. The sample was mounted at the end of the cold finger of a closed-cycle cryogenic refrigerator with the (HHL) plane coincident with the scattering plane. Measurements of charge peaks showed no indications for changes of the structure and the crystallographic symmetry through the magnetic transition.

For temperatures above $T_N = 8.5$ K, only Bragg peaks consistent with the chemical structure[22,23] of GdBiPt were observed. However, upon cooling below T_N, additional Bragg scattering at half-integer values of (HKL) was found as shown in Fig. 2(a). The magnetic origin of these peaks was confirmed by energy scans through the Gd L_2 absorption edge and from the temperature dependence of the diffraction peak intensity as described below.

The energy scan in Fig. 2(b) was performed with the diffractometer set at the magnetic peak position and is typical of resonant magnetic scattering at the L edges of rare-earth compounds.[26] At the L_2 edge of rare-earth elements, the resonance primarily involves electric dipole ($E1$) transitions from the $2p_{\frac{1}{2}}$ core level to the empty $5d$ states, seen as the strong line just at, or slightly below, the maximum in the measured fluorescence intensity. The weaker feature below the $E1$ resonance in Fig. 2(b) is likely due to the electric quadrupole ($E2$) transition from the $2p_{\frac{1}{2}}$ core level to the $4f$ states that are pulled below the Fermi energy because of the presence of the core hole in the resonance process.

The temperature dependence of the magnetic scattering, along with the corresponding magnetization measurements performed on a sample from the same batch using a Quantum Design Magnetic Properties Measurement System, are shown in Fig. 3. The magnetic order parameter was measured at the $(\frac{1}{2}\frac{1}{2}\frac{9}{2})$ peak position as the sample temperature was increased during a temperature scan in the absence of the polarization analyzer. These data were supplemented by measurements of the integrated intensity of the $(\frac{1}{2}\ -\frac{1}{2}\ \frac{13}{2})$ magnetic Bragg peak at selected temperatures and with polarization analysis. The line in Fig. 3(b) describes a fit to the integrated intensity data using a power law of the form $I \sim (1 - \frac{T}{T_N})^{2\beta}$, yielding $T_N = 8.52 \pm 0.05$ K and $\beta = 0.33 \pm 0.02$. The close proximity of

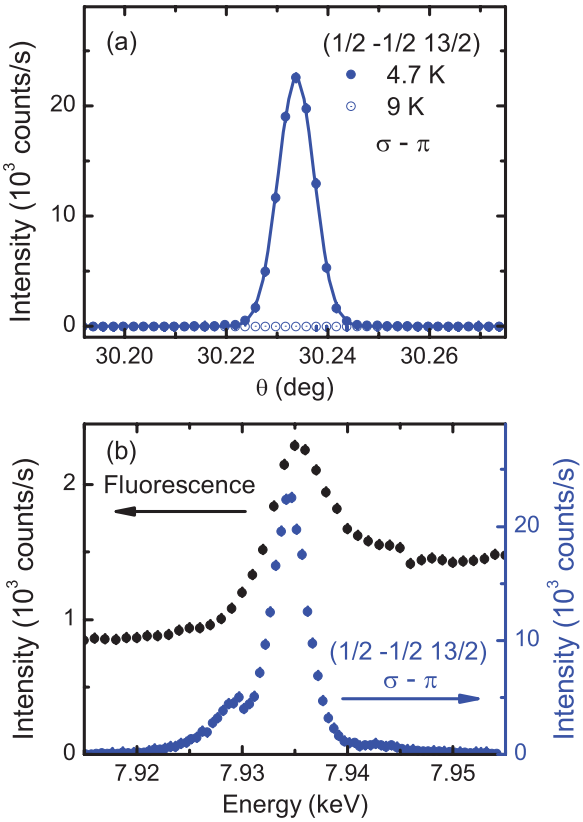

FIG. 2. (Color online) Resonant magnetic scattering from the GdBiPt single crystal. (a) Rocking scans (θ) through the $(\frac{1}{2}\ -\frac{1}{2}\ \frac{13}{2})$ magnetic peak position above (open circles) and below (solid circles) T_N taken in σ-π scattering geometry using the PG (006) analyzer. (b) Energy scan through the Gd L_2 absorption edge at the $(\frac{1}{2}\ -\frac{1}{2}\ \frac{13}{2})$ magnetic peak position at $T = 4.7$ K (blue/gray solid circles) along with the measured x-ray fluorescence from the sample (black solid circles).

T_N determined from our scattering measurements and the peak in $d[(M/H)T]/dT$ (Ref. 27) at $T = 8.6$ K again confirms the magnetic origin of the Bragg scattering with a propagation vector of $\mathbf{q}_m = (\frac{1}{2}\frac{1}{2}\frac{1}{2})$. Systematic M vs H measurements (not shown) demonstrate, in addition, that no spontaneous ferromagnetic moment is present.

Having established the nature of the magnetic ordering in GdBiPt, we now describe our attempt to determine the direction of the ordered magnetic moment. The angular dependence of the resonant magnetic intensity $I(\psi)$ for the incident σ-polarized beam depends upon the component of the magnetic moment along the scattered beam direction and can be written as $I(\psi)_{(\mathbf{Q},\alpha,\beta)} = C[\widehat{\mathbf{m}} \cdot \widehat{\mathbf{k}'}(\psi)_{(\mathbf{Q})}]^2 A(\psi)_{(\mathbf{Q},\alpha,\beta)}$, where C is an overall scale factor that accounts for the resonant scattering matrix element and incident beam intensity, $\widehat{\mathbf{m}}$ and $\widehat{\mathbf{k}'}$ represent the magnetic moment and scattered beam directions, respectively, and A accounts for the absorption correction.[28] The sample geometry required off-specular scattering measurements of the magnetic peaks. That is, the angle α of the incident beam $\mathbf{k}$ with respect to the sample surface is different from the angle β of the outgoing beam $\mathbf{k}'$ with respect to the sample surface.[29] For the azimuth angle ψ scans shown in Fig. 4, the diffractometer was set at the position of the

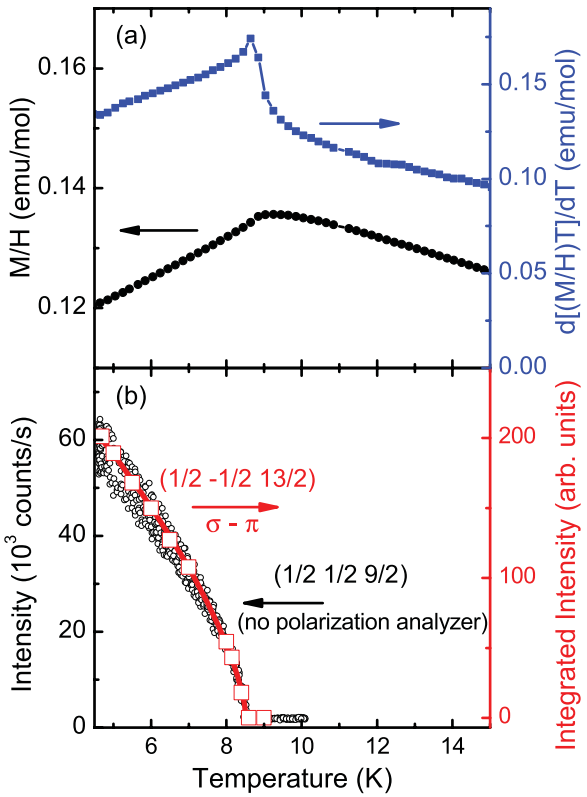

FIG. 3. (Color online) (a) M/H and its temperature derivative for GdBiPt. (b) The magnetic intensity measured while scanning temperature at the maximum of the $(\frac{1}{2}\,\frac{1}{2}\,\frac{9}{2})$ diffraction peak without a polarization analyzer (open small circles) and the integrated intensity of the $(\frac{1}{2}\ -\frac{1}{2}\,\frac{13}{2})$ diffraction peak measured at selected temperatures using the polarization analyzer (open large squares). The solid line is a power-law fit to the integrated intensity data as described in the text.

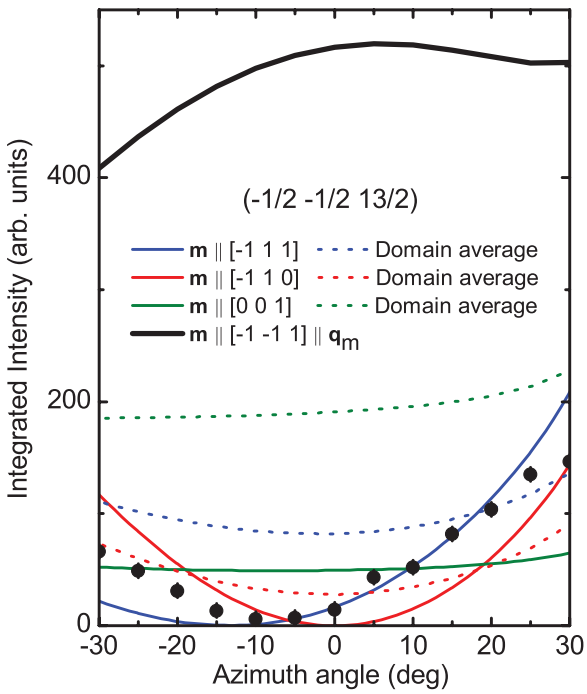

FIG. 4. (Color online) Integrated intensity in azimuth scans through the $(-\frac{1}{2}\ -\frac{1}{2}\,\frac{13}{2})$ magnetic Bragg peak. Measured data are depicted by solid black circles. Solid and dashed lines represent calculations for selected magnetic moment directions in a single magnetic domain, and for intensity from equally populated domains averaged over the three possible symmetry-equivalent magnetic moment orientations, respectively.

magnetic Bragg peak and the crystal was rotated about the scattering vector $\mathbf{Q} = \mathbf{k}' - \mathbf{k}$, thereby rotating $\widehat{\mathbf{k}}'$ with respect to $\widehat{\mathbf{m}}$ while leaving $\mathbf{Q}$ fixed. This yields an azimuth dependence of the intensity which is specific to a given magnetic moment direction. Note that the absorption correction A also depends on the azimuth angle ψ.

For a cubic lattice, the determination of the ordered moment direction is generally not possible due to the presence of domains that arise from symmetry-equivalent magnetic propagation vectors and moment directions. For the observed magnetic Bragg peaks at (HKL) with H, K, and L half integers, four symmetry-equivalent $\{\frac{1}{2}\,\frac{1}{2}\,\frac{1}{2}\}$ propagation vectors exist: $(-\frac{1}{2}\ -\frac{1}{2}\,\frac{1}{2})$, $(\frac{1}{2}\ -\frac{1}{2}\ -\frac{1}{2})$, $(-\frac{1}{2}\,\frac{1}{2}\ -\frac{1}{2})$, and $(\frac{1}{2}\,\frac{1}{2}\,\frac{1}{2})$. Fortunately, for GdBiPt in the cubic space group $F\bar{4}3m$, only one propagation vector contributes to a particular magnetic reflection as a consequence of the face-centered symmetry, and thus allows some further insight into the magnetic moment direction [e.g., the magnetic Bragg peak $(-\frac{1}{2}\ -\frac{1}{2}\,\frac{13}{2})$ is generated by the propagation vector $\mathbf{q}_m = (-\frac{1}{2}\ -\frac{1}{2}\,\frac{1}{2})$ from the (006) zone center]. The measured data for the $(-\frac{1}{2}\ -\frac{1}{2}\,\frac{13}{2})$ magnetic Bragg peak show two important features in the azimuth scan presented in Fig. 4: a distinct minimum with almost no intensity close to $\psi = 0$, and an increase in intensity by more than an order of magnitude as ψ is varied by $\pm 30^\circ$. Both features are in strong contrast to the expected ψ dependence of the intensity for magnetic moments parallel to the propagation vector $\mathbf{q}_m = (-\frac{1}{2}\ -\frac{1}{2}\,\frac{1}{2})$, as illustrated in Fig. 4 by the bold black line with a maximum close to $\psi = 0$. Therefore, we can exclude that the moments are parallel to the propagation vector in GdBiPt.

In Fig. 4, calculated curves are also shown for other moment directions. However, for each of the depicted moment directions, three different symmetry-equivalent moment orientations can occur yielding three magnetic domains. The dashed lines in Fig. 4 represent the calculated ψ dependence of the intensity if we include all such domains with equal population and note that the same dashed curves would be obtained from a noncollinear magnetic structure (e.g., a cycloidal ordering of magnetic moments along the same direction oscillating about the propagation vector). We again find poor agreement between these calculations for moments along the set of $\{-111\}$,$\{-110\}$, and $\{001\}$ directions. However, calculations assuming the presence of only a single domain within the probed volume, with one specified collinear moment direction [either $[-111]$ or $[-110]$ for the $(-\frac{1}{2}\ -\frac{1}{2}\,\frac{13}{2})$ Bragg peak in Fig. 4], come much closer to describing the measured data. However, since the probed scattering volume contains more than one type of magnetic moment direction domains, no single curve in Fig. 4 provides a fully satisfying fit to the data. Azimuthal scans through other magnetic peaks at $(\pm\frac{1}{2}\ \pm\frac{1}{2}\,\frac{13}{2})$ positions yield similar results. This behavior indicates that (i) the measured azimuthal dependence results from averaging

over only a limited number of moment direction domains, and (ii) the magnetic domains are sizable but somewhat smaller than the footprint of the incident beam on the sample ($\sim 0.5 \times 0.5$ mm^2). Similar large magnetic domains have been noted in previous XRMS work on $GdNi_2Ge_2$ as well.[30] Nevertheless, a unique determination of the moment direction is not possible based on the available data, but may be feasible from measurements using much smaller incident beam dimensions and/or control of domain populations through an applied magnetic field or applied stress.[30]

Summarizing the experimental results, below $T_N = 8.5$ K the magnetic Gd moments order in a commensurate antiferromagnetic structure in GdBiPt that can be described as doubling the cubic unit cell along the diagonal [111] direction, so that alternating ferromagnetic (111) planes of Gd are antiferromagnetically coupled along the [111] direction. The moments are not aligned parallel to this diagonal [111] direction. In contrast to GdBiPt, CeBiPt is an antiferromagnet characterized by a propagation vector $\mathbf{q}_m = (100)$ and the ordered moments are collinear with the propagation vector along [100],[6] but with a reduced moment that may, in part, be attributed to crystalline electric field (CEF) effects.[31] Unfortunately, XRMS measurements do not allow a direct extraction of the ordered moment in GdBiPt, but earlier specific-heat measurements[2] estimated an entropy of $\sim 0.8\mathcal{R} \ln 8$ associated with the magnetic transition close to the value expected for full moment ordering without CEF effects. The entropy associated with the corresponding magnetic transitions for the Nd, Tb, and Dy compounds were considerably less than $\mathcal{R} \ln(2J + 1)$ expected for the full Hund's rule J multiplet, indicating the importance of CEF effects in these compounds. The magnetic structures for $R =$ Nd, Sm, Tb, Dy, Ho, Er, Tm, and Yb have not yet been identified by neutron or XRMS measurements and such measurements are planned.

Finally, we comment on our results in light of the proposal that GdBiPt may be an AFTI candidate.[20] The magnetic structure determined here is consistent with the model B presented by Mong *et al.*,[20] where the AFTI state may be derived from spin-orbit coupling induced by this specific antiferromagnetic ordering. The doubling along the cubic diagonal direction represents the broken lattice translational symmetry (by an order of two) and the magnetic ordering breaks the time-reversal symmetry, however, the product of both symmetry operations is conserved for the determined magnetic order. In light of this, additional ARPES measurements for $T < T_N$ are needed to fully address the question whether the electronic structure of GdBiPt in the antiferromagnetic state fulfills the other conditions[20] necessary for an AFTI.

We acknowledge valuable discussions with A. Kaminski, J. E. Moore, R. S. K. Mong, P. J. Ryan, and J. C. Lang. This work was supported by the Division of Materials Sciences and Engineering, Office of Basic Energy Sciences, US Department of Energy. Ames Laboratory is operated for the US Department of Energy by Iowa State University under Contract No. DE-AC02-07CH11358. Use of the Advanced Photon Source was supported by the US DOE under Contract No. DE-AC02-06CH11357.

[1] T. Graf, S. S. P. Parkin, and C. Felser, IEEE Trans. Magn. **47**, 367 (2011).
[2] P. C. Canfield, J. D. Thompson, W. P. Beyermann, A. Lacerda, M. F. Hundley, E. Peterson, Z. Fisk, and H. R. Ott, J. Appl. Phys. **70**, 5800 (1991).
[3] G. Goll, M. Marz, A. Hamann, T. Tomanic, K. Grube, T. Yoshino, and T. Takabatake, Physica B **403**, 1065 (2008).
[4] N. P. Butch, P. Syers, K. Kirshenbaum, A. P. Hope, and J. Paglione, e-print arXiv:1109.0979.
[5] Z. Fisk *et al.*, Phys. Rev. Lett. **67**, 3310 (1991).
[6] J. Wosnitza *et al.*, New J. Phys. **8**, 174 (2006).
[7] S. Chadov, X. Qi, J. Kübler, G. H. Fecher, C. Felser, and S. C. Zhang, Nat. Mater. **9**, 541 (2010).
[8] H. Lin, L. A. Wray, Y. Xia, S. Xu, S. Jia, R. J. Cava, A. Bansil, and M. Z. Hasan, Nat. Mater. **9**, 546 (2010).
[9] D. Xiao, Y. Yao, W. Feng, J. Wen, W. Zhu, X.-Q. Chen, G. M. Stocks, and Z. Zhang, Phys. Rev. Lett. **105**, 096404 (2010).
[10] C. Li, J. S. Lian, and Q. Jiang, Phys. Rev. B **83**, 235125 (2011).
[11] L. Fu and C. L. Kane, Phys. Rev. B **76**, 045302 (2007).
[12] D. Hsieh, D. Qian, L. Wray, Y. Xia, Y. S. Hor, R. J. Cava, and M. Z. Hasan, Nature (London) **452**, 970 (2008).
[13] Y. Xia *et al.*, Nat. Phys. **5**, 398 (2009).
[14] H. Zhang, C. X. Liu, C. L. Qi, X. Dai, Z. Fang, and S. C. Zhang, Nat. Phys. **5**, 438 (2009).
[15] Y. L. Chen *et al.*, Science **325**, 178 (2009).
[16] M. Z. Hasan and C. L. Kane, Rev. Mod. Phys. **82**, 3045 (2010).
[17] J. E. Moore, Nature (London) **464**, 194 (2010).
[18] R. Li, J. Wang, X.-L. Qi, and S.-C. Zhang, Nat. Phys. **6**, 284 (2010).
[19] P. Hosur, S. Ryu, and A. Vishwanath, Phys. Rev. B **81**, 045120 (2010).
[20] R. S. K. Mong, A. M. Essin, and J. E. Moore, Phys. Rev. B **81**, 245209 (2010).
[21] C. Liu, Y. Lee, T. Kondo, E. D. Mun, M. Caudle, B. N. Harmon, S. L. Bud'ko, P. C. Canfield, and A. Kaminski, Phys. Rev. B **83**, 205133 (2011).
[22] A. E. Dwight, in *Proceedings of the 11th Rare Earth Research Conference*, edited by J. M. Haschke and H. A. Eick (US Atomic Energy Commission, Washington, DC, 1974), Vol. 2, p. 642.
[23] R. A. Robinson, A. Purwanto, M. Kohgi, P. C. Canfield, T. Kamiyama, T. Ishigaki, J. W. Lynn, R. Erwin, E. Peterson, and R. Movshovich, Phys. Rev. B **50**, 9595 (1994).
[24] R. H. Forster, G. B. Johnston, and D. A. Wheeler, J. Phys. Chem. Solids **29**, 855 (1968).
[25] P. C. Canfield and Z. Fisk, Philos. Mag. B **65**, 1117 (1992).
[26] J. W. Kim, Y. Lee, D. Wermeille, B. Sieve, L. Tan, S. L. Bud'ko, S. Law, P. C. Canfield, B. N. Harmon, and A. I. Goldman, Phys. Rev. B **72**, 064403 (2005).
[27] M. E. Fisher, Philos. Mag. **82**, 1731 (1962).
[28] C. Detlefs, A. H. M. Z. Islam, A. I. Goldman, C. Stassis, P. C. Canfield, J. P. Hill, and D. Gibbs, Phys. Rev. B **55**, R680 (1997).
[29] H. You, J. Appl. Crystallogr. **32**, 614 (1999).
[30] J. W. Kim, A. Kreyssig, L. Tan, D. Wermeille, S. L. Bud'ko, P. C. Canfield, and A. I. Goldman, Appl. Phys. Lett. **87**, 202505 (2005).
[31] G. Goll, O. Stockert, M. Prager, T. Yoshino, and T. Takabatake, J. Magn. Magn. Mater. **310**, 1773 (2007).